Structure, Vol. 12, 987–998, June, 2004, ©2004 Elsevier Ltd. All rights reserved. DOI 10.1016/j.str.2004.03.024

The Structure of the N-Terminal Domain of the Product of the Lissencephaly Gene *Lis1* and Its Functional Implications

Myung Hee Kim,[1] David R. Cooper,[1] Arkadiusz Oleksy,[2] Yancho Devedjiev,[1] Urszula Derewenda,[1] Orly Reiner,[3] Jacek Otlewski,[2] and Zygmunt S. Derewenda[1,*]

[1]Department of Molecular Physiology and Biological Physics and Cancer Center
University of Virginia
Charlottesville, Virginia 22908

[2]Laboratory of Protein Engineering
Institute of Biochemistry and Molecular Biology
University of Wroclaw
Tamka 2, 50-137 Wroclaw
Poland

[3]Department of Molecular Genetics
Weizmann Institute of Science
76100 Rehovot
Israel

Summary

Mutations in the *Lis1* gene result in lissencephaly (smooth brain), a debilitating developmental syndrome caused by the impaired ability of postmitotic neurons to migrate to their correct destination in the cerebral cortex. Sequence similarities suggest that the LIS1 protein contains a C-terminal seven-blade β-propeller domain, while the structure of the N-terminal fragment includes the LisH (Lis-homology) motif, a pattern found in over 100 eukaryotic proteins with a hitherto unknown function. We present the 1.75 Å resolution crystal structure of the N-terminal domain of mouse LIS1, and we show that the LisH motif is a novel, thermodynamically very stable dimerization domain. The structure explains the molecular basis of a low severity form of lissencephaly.

Introduction

The formation of a normal human cerebral cortex depends on the precise migration of billions of neurons from the ventricular zone to their final destinations in one of the six layers of gray matter, the seat of all higher functions of the brain. Any impairment of this complex process has debilitating consequences, and disorders of neuronal migration account for the most commonly observed developmental neurological syndromes (Ross and Walsh, 2001). Two such severe disorders include lissencephaly, or "smooth brain" (Morris, 2000) and subcortical band heterotopia, or "double cortex" (Berg et al., 1998). In these genetic diseases the neurons either fail to migrate to the cortex, creating disorganized cortical layers, i.e., lissencephaly, or accumulate inappropriately within the white matter resulting in apparent additional layers, leading to the so-called double cortex syndrome. Lissencephaly leads to severe mental retardation and early death, while the double cortex syndrome is typically X linked and found in female patients.

Recent progress in human genetics of developmental brain disorders helped to identify the putative causal genes. Lissencephaly and the double cortex syndromes have been explicitly associated with mutations in the *Lis1* and *DCX* genes, respectively (Gleeson et al., 1998; des Portes et al., 1998; Reiner et al., 1993). However, neither the molecular functions of these proteins nor the exact roles they play in directing neuronal migration are understood. Doublecortin was shown to be a microtubule-associated protein (MAP) containing a tandem repeat of homologous DCX domains (Sapir et al., 2000; Taylor et al., 2000; Horesh et al., 1999; Gleeson et al., 1999; Francis et al., 1999). We recently showed that DCX domains, found also in several other proteins and in genomes of some lower eukaryotes, have a ubiquitin-like tertiary fold and bind to tubulin and/or microtubules (Kim et al., 2003). While not proven to be a canonical MAP, LIS1 also influences the microtubule-linked cellular functions, such as neuronal migration, dynein regulation during mitotic cell division, and chromosomal segregation, via possible interactions with tubulin (Sapir et al., 1997), cytoplasmic dynein (Faulkner et al., 2000; Smith et al., 2000), CLIP-170 (Coquelle et al., 2002), and NudE and NudeL (Sasaki et al., 2000; Kitagawa et al., 2000; Feng et al., 2000; Niethammer et al., 2000). LIS1 was also identified as a noncatalytic subunit of the heterotrimeric platelet-activation factor acetylhydrolase (PAF-AH), which regulates the level of the powerful lipid messenger platelet-activation factor (PAF) in the brain by converting it to the biologically inactive lyso-PAF (Hattori et al., 1996). The optimal level of PAF in the embryonic brain appears to be required for precise neuronal migration, but the mechanism by which PAF regulates neuronal migration is unclear (Albrecht et al., 1996). Recent evidence suggests that both PAF receptor-dependent and receptor-independent pathways are involved and that LIS1 plays a key role in the latter (Tokuoka et al., 2003).

Orthologs of LIS1 have been identified in numerous eukaryotic genomes, ranging from the *Saccharomyces cerevisiae* (Geiser et al., 1997), *Aspergillus nidulans* (Xiang et al., 1995), *Caenorhabditis elegans* (Dawe et al., 2001), and *Drosophila melanogaster* (Sheffield et al., 2000) to mammals. The sequences are highly conserved, suggesting a crucial biological function, and homozygous *Lis1* knockouts are lethal. In *A. nidulans* and *C. elegans* the proteins have a documented function in nuclear migration, and this may also be a mechanism by which LIS1 is involved in neuronal migration. Further, LIS1 was shown to play a critical role in the genetic union in the fertilized mammalian oocyte (Payne et al., 2003), while inactivation of testis-specific LIS1 causes male infertility (Nayernia et al., 2003).

The protein sequence of LIS1 contains three distinct regions. The N-terminal so-called LIS1-homology motif (LisH) which includes residues 1–39 has been recently

*Correspondence: zsd4n@virginia.edu

recognized as a novel ubiquitous motif, found in 114 eukaryotic proteins, suggesting a common function (Emes and Ponting, 2001). The fragment spanning amino acids 40–85 was predicted to be a coiled-coil region. Together, LisH and the coiled-coil fragments are involved in homodimerization of the protein, although the presence of the coiled coil is not critical (Tai et al., 2002). Finally, the seven C-terminal WD40 repeats (residues 96–410) suggest that the main domain of LIS1 is a β-propeller structure first identified in the β subunit of heterotrimeric G proteins, but also found in hundreds of other human noncatalytic proteins either alone or with domains of other types fused to its N terminus (Neer et al., 1994).

Although the WD40 domain of LIS1 is thought to mediate most of the latter's interactions with other proteins described in the literature, the N-terminal domain containing the LisH motif and the putative coiled-coil fragment is also important for the protein's physiological function. An N-terminal deletion mutant of LIS1 results in an aberrant morphology for cortical neurons and radial glia in the developing cortex, with a concomitant retardation of neuronal migration (Cahana et al., 2001). To better understand the structure and function of the N-terminal domain of LIS1, and to gain insight into the potential function of the LisH motif, we determined the crystal structure of the recombinant fragment encompassing residues 1–86 of the mouse ortholog of LIS1, and we refined the atomic model at 1.75 Å resolution. We show, that the LisH domain constitutes a novel and previously unknown homodimerization motif, located, as predicted, adjacent to a coiled-coil fragment. Surprisingly, the homodimer shows rare asymmetry, with possible functional consequences.

Results

Structure Solution and Quality of the Model

A construct corresponding to the N-terminal domain of mouse LIS1 (residues 1–86), which we refer to henceforth as N-LIS1, was expressed in *E. coli*, and purified and crystallized as described in Experimental Procedures. A multiwavelength anomalous dispersion (MAD) experiment was conducted using SeMet-labeled crystals. The model was refined at 1.75 Å (Table 1) and contains four copies of N-LIS1 in the asymmetric unit. A total of 311 out of the 352 expected residues are included in the model, with the missing residues located at the N- or C termini of all four monomers. Only three side chains are not visible in the σ_A weighted $2mF_{obs}$-DF_{calc} electron density map contoured at 1σ (Figure 1A). The refined structure conforms well to standard protein stereochemistry with rms deviation from ideal bond lengths of 0.016 Å, and no residues fall into disallowed regions of the Ramachandran plot as judged by MolProbity (Lovell et al., 2002). The average isotropic temperature factor (*B*) for main chain atoms is 20.2 Å^2, with the highest temperature factors associated with N- and C termini and a short helix at the most extended portion of the LisH motif. These regions, which are completely contained within the electron density, are involved in or are adjacent to areas of crystallographic contacts.

The Overall Structure of N-LIS1

The asymmetric unit of the crystal contains four N-LIS1 molecules associated into two homodimers (denoted A/B and C/D). While the homodimers, related by a noncrystallographic dyad, are very similar, the two molecules within each dimer surprisingly reveal significant conformational differences, so that molecules A and C resemble each other but are different from B and D, which are also alike. Thus, within the homodimer there is a significant deviation from the expected local 2-fold symmetry. The two molecules in each of the homodimers are aligned in general terms in a parallel fashion, forming a structure resembling a mallet. The head of the mallet is formed by the two LisH motifs, each containing, as predicted (Emes and Ponting, 2001), two α helices (α_1, residues 5–21, and α_2, residues 25–34), and also a segment comprising residues Glu36–Tyr47 and crossing over the two helices on the outside face of the LisH dimer, connecting to the C-terminal coiled-coil portion (Figures 1B and 1C).

The handle of the mallet is made up of two C-terminal α helices, contributed from each of the two molecules, starting at residue 50, which form a parallel coiled coil. However, while the N termini of the helices are fixed at approximately 55° angle to each other, their parallel disposition is only made possible by a severe kink in one of the helices at residues Thr56 and Ser57 (Figure 2). Amino acid sequence comparisons of known LIS1 orthologs, and other proteins containing the LisH motif, reveal sequence conservation patterns consistent with the structural model obtained for N-LIS1 (Figure 3).

LisH: A Novel Homodimerization Domain

The two LisH motifs create a novel antiparallel four-helix bundle, with no significant matches identified by either DALI (Holm and Sander, 1997) or VAST (Gibrat et al., 1996). The homodimerization of the LisH motif is accomplished exclusively by the two N-terminal helices, α_1 and α_2, which collectively bury 1800 Å^2 per monomer of mostly hydrophobic surface. The interface between the monomers is tightly packed with Ile15, Tyr18, Leu19, Tyr24, and Phe31 forming the core hydrophobic cluster. All five amino acids are completely conserved among vertebrates in all known LIS1 sequences, and Tyr18, Leu19, and Phe31 are among the few most-conserved amino acids in the LisH motif. The antiparallel interaction of the α_2 helices (residues 25–34) is also stabilized by Glu34 of each helix capping the backbone amides of Glu26 and Ala27 in the second helix across the interface (Figure 4A). Consistent with this important structural role, Glu34 is completely conserved among all known LIS1 proteins, and is nearly invariant among the LisH motifs (Figure 3). Compared to the intermolecular interface, the packing of the α_1 against the α_2 helix within each individual molecule appears less well defined (Figure 4B), suggesting that the tertiary structure of the LisH motif is sustained predominantly by the dimerization.

The next fragment of the molecule, extending from the end of α_2 to the coiled-coil motif, contains an extended structure (residues Glu36–Asn40), a highly solvent-exposed loop comprised of Asn40, Glu41, and Glu42, another short helix (α_3), Leu43-Tyr47, and an irregular

Table 1. Data Collection and Refinement Statistics

Crystal			
Space group	$P2_12_12$		
Unit cell (Å)	a = 63.0, b = 111.7, c = 47.4		
Data Collection Statistics			
	Edge	Peak	Remote
Wavelength (Å)	0.97953	0.97939	0.96422
Resolution (Å)[a]	40.0–1.75 (1.81–1.75)	40.0–2.30 (2.38–2.30)	40.0–1.75 (1.81–1.75)
Total reflections	213,432	67,121	212,295
Unique reflections	33,179	15,168	32,510
Redundancy	6.4	4.4	6.5
Completeness (%)[a]	94.9 (74.7)	97.0 (81.6)	93.3 (63.1)
R_{sym}[a,b] (%)	5.4 (40.1)	4.5 (8.7)	5.2 (51.1)
I/σ (I)[a,b]	42.7 (1.4)	27.3 (9.8)	28.1 (1.9)
Phasing Statistics			
Phasing power[c], iso/ano	–/1.77	0.89/0.78	1.19/0.78
R_{cullis}[d], iso/ano	–/0.64	0.67/0.77	0.66/0.80
Figure of merit (acentric)		0.36	
Refinement Statistics			
Resolution (Å)		40.0–1.75	
Reflections (working)		31,827	
Reflections (test)		1,069	
R_{work} (%)[e]		19.0	
R_{free} (%)[e]		24.4	
Number of waters		183	
Rms deviation			
Bond lengths (Å)		0.016	
Bond angles (°)		2.84	
Average *B* factor (Å^2)			
Main chain		20.2	
Side chain		24.8	
Waters		43.3	

[a] Values in parentheses correspond to the last shell.
[b] $R_{sym} = \Sigma|I_i - \langle I\rangle|/\Sigma I$, where I_i is the intensity of the i-th observation and $\langle I\rangle$ is the mean intensity of the reflections. The values are for unmerged Friedel pairs.
[c] Phasing power = rms($|F_h|/E$), where $|F_h|$ is the heavy atom structure factor amplitude and E is residual lack of closure error.
[d] $R_{cullis} = \Sigma||F_{h.obs}| - ||F_{h.calc}||/\Sigma|F_h|$ for acentric reflections, where $|F_{h.obs}|$ is the observed heavy atom structure factor amplitude and $|F_{h.calc}|$ is the calculated heavy atom structure factor amplitude. [e] $R_{work} = \Sigma||F_{obs}| - |F_{calc}||/\Sigma|F_{obs}|$, crystallographic R factor, and $R_{free} = \Sigma||F_{obs}| - |F_{calc}||/\Sigma|F_{obs}|$, where all reflections belong to a test set of randomly selected data.

dipeptide Ala48 and Gly49 immediately prior to the C-terminal helix (α_4). This fragment has few contacts with the LisH helical motif, and its structure seems to be mostly maintained by polar interactions and particularly the hydrogen bonds involving the side chains of Arg13 and Asp44 with the backbone carbonyl of Asp38 and the amides of Glu41 and Asn40. The segments cross the LisH motif of the outside of the mallet's "head," are highly solvent exposed, and are involved in crystal contacts. A comparison of the four molecules reveals small but significant conformational differences between them, easily attributed to crystal packing forces. Helix α_3 has some of the highest *B* factors of the structure. It is loosely formed, with one of the four monomers showing a 3_{10} stereochemistry, two monomers showing a mix of α helix and a 3_{10} helix, and one with a true α helix.

It is not clear whether the bridging segment should be regarded as an integral part of an extended LisH domain or if it is a mere linker. Additional structure determinations of homologous domains from other proteins will be required to address this issue. It is clear, however, from the sequence alignment, that this is the least evolutionarily conserved fragment of N-LIS1.

The Coiled-Coil Fragment

Following Gly49, both molecules form a helix (α_4), which in molecules C and D continues until residue 79, the last residue visible in electron density. The axes of the N termini of the α_4 helices are fixed at $\sim$55° with respect to each other, and this conformation seems largely defined by the packing of the indole group of Trp55 against the LisH motif. Uninterrupted, the two helices would cross each other and form an "open scissors" structure (Figure 2A). However, in molecules A and C, the helix breaks after two turns to form a sharp kink involving Thr56 and Ser57. Both of these residues have strained secondary structures outside the canonical helical regions ($\varphi \approx 105°$, $\psi \approx 15°$, and $\varphi \approx 105°$, $\psi \approx -10°$, respectively, in both A and C chains), and the remaining portion of the helix in molecules A and D becomes aligned with the counterpart from B and D, respectively, to form a parallel coiled-coil structure, which becomes

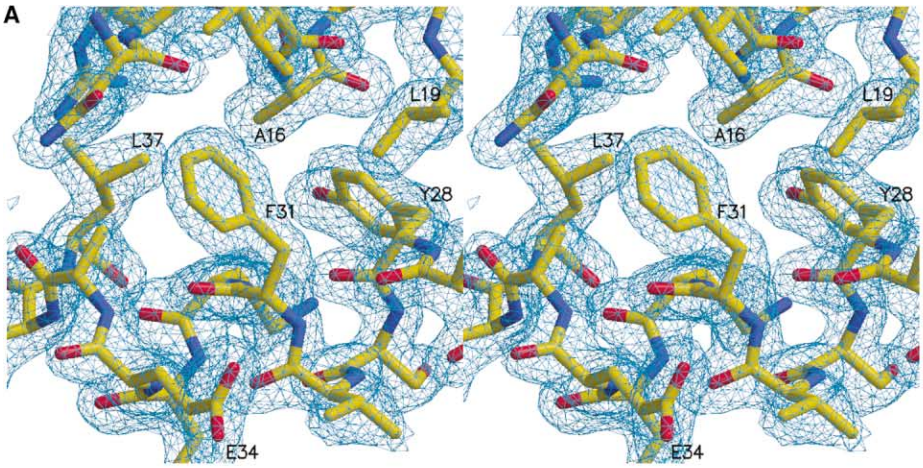
A
L19
L37
A16
F31
Y28
E34
L19
L37
A16
F31
Y28
E34

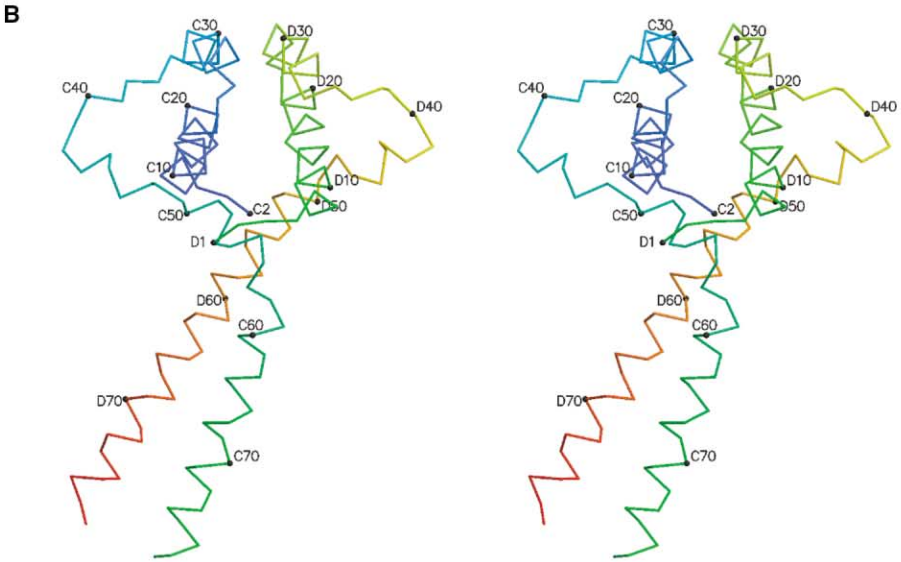
B
C30
D30
C40
C20
D20
D40
C10
D10
C50
C2
D50
D1
D60
C60
D70
C70
C30
D30
C40
C20
D20
D40
C10
D10
C50
C2
D50
D1
D60
C60
D70
C70

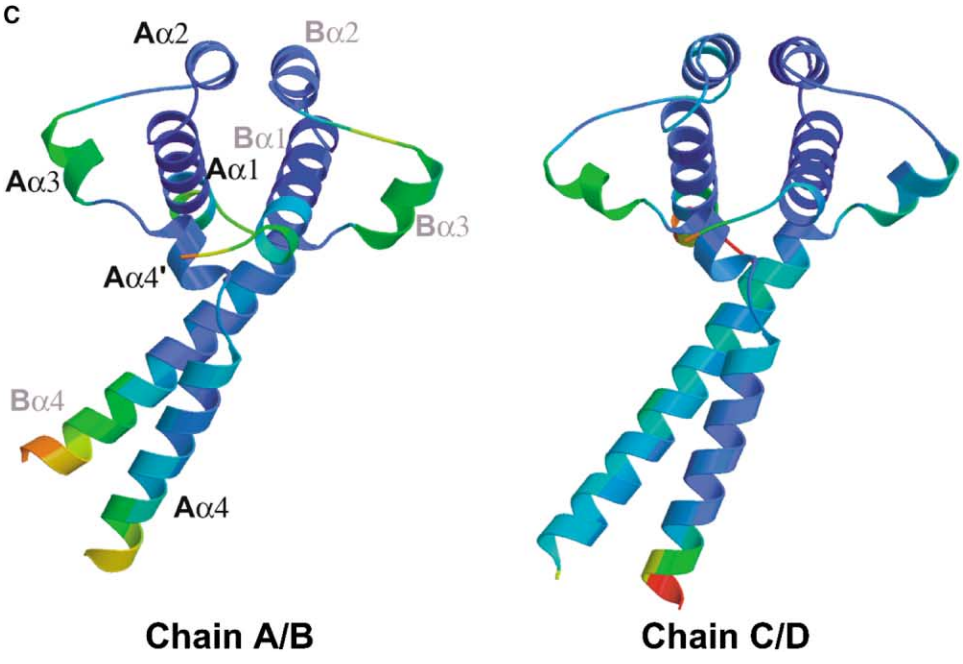
C
Aα2
Bα2
Bα1
Aα1
Aα3
Bα3
Aα4'
Bα4
Aα4
Chain A/B
Chain C/D

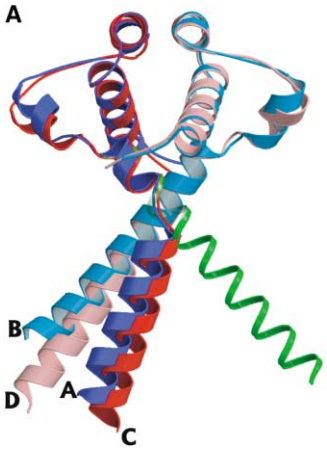

Figure 2. Superpositions of N-LIS1

(A) Superposition of the A/B dimer in blue and cyan onto the C/D dimer in red and pink, respectively. The thin green helix is a hypothetical model of how chain C would extend if it were not kinked.

(B) Superposition of the C monomer on the D monomer. The capital letters indicate chain names.

the "handle" of "broken" mallet, in which the head appears twisted away from its expected position (Figure 5).

Following the kink segment, Val58 initiates the first of three nearly canonical heptad repeats characteristic of a coiled-coil structure: VIRLQKK/VMELESK/LNEAKEE (Figure 3B). In a typical heptad, *abcdefg* (Gruber and Lupas, 2003), the *a* and *d* residues have hydrophobic side chains that make up the interhelical zipper, while *e* and *g* carry opposite charges that provide electrostatic stabilization. The interface between the two α_4 helices of N-LIS1 is formed by Val58, Leu61, Val65, Leu68, and Leu72, found in the *a* and *d* sites of the first and second repeat and site *a* of the third, respectively (alanine occupies site *d*). Both the second and third repeat also provide classical electrostatic interactions (E-K and K-E), although in the first repeat Gln62 is found in the position where Glu is expected. The incomplete hydrophobic interaction in the third heptad probably explains why the two helices begin to part at that point and their C-terminal portions are no longer ordered in the crystal structure (Figure 5).

The first two heptads preserve nearly identical sequences throughout evolution, with the exception of just a few very conserved substitutions in *A. nidulans* and *C. elegans*. This pattern of conservation fades rapidly downstream, and the amino acid sequences beyond the three heptads no longer show coiled-coil characteristics, but instead, we observe a preponderance of glycines and prolines. The ends of the α_4 helices in all four monomers have some of the higher *B* factors observed in this crystal structure, and although the expressed protein contained residues 1–86, density is only present up to Phe79 in two chains, Glu77 in one chain, and Ala75 in the last monomer. We infer from these data that residues between ~80 and 100 are likely to constitute a flexible linker making it possible to pack two large WD40 β-propeller domains at the end of the dimerization motif.

The Stability of the N-LIS1 Homodimer

Size-exclusion chromatography shows that the N-LIS1 fragment is dimeric in solution in a broad range of concentration from 1 to 50 μM (data not shown). To assess the stability of the N-LIS1 homodimer, and to evaluate the apparent dissociation constant, we monitored chemically induced unfolding of the protein by fluorescence and by circular dichroism (CD) (Figure 6A). In both cases the reaction follows a single and coincident transition, which suggests that only two states are significantly populated in the unfolding transition: the native dimer and the unfolded monomer (Bowie and Sauer, 1989). We ruled out the possibility that the homodimer dissociates into native monomers before unfolding, since in such a case the unfolding reaction would be unimolecular and protein concentration independent. Since the midpoint of the unfolding transition ($[GdmCl]_{1/2}$) clearly depends on the protein concentration, the dimer is thermodynamically favored at higher protein concentrations (Neet and Timm, 1994). The free energy change of unfolding ($\Delta G_u^{H_2O}$) is very high, $\cong$22 kcal/mol mol^{-1} (~90 kJ mol^{-1}, see Table 2), which corresponds to an apparent dissociation constant K_d lower than 10^{-15} M. Dimeric proteins with stabilities exceeding 85 kJ mol^{-1} are thought to be stable at physiological concentrations below 10 pM (Neet and Timm, 1994). At high denaturant concentrations the ellipticity drops essentially to zero, which means that unfolded monomers do not have any stable helical fragments. A similar picture of LIS1 unfolding/dissociation is observed in thermal unfolding experiments, although in this case about 10% of residual structure is preserved in the unfolded state at elevated temperatures (data not shown). Additionally, we found that the mean residue ellipticity at 222 nm shows no change with protein concentration in 0.5–4 μM range, indicating that the dimer is stable and does not dissociate into partially or fully folded monomers (Figure 6B).

Figure 1. Overall Structure of Dimeric N-LIS1 Showing a Mallet Shape

(A) Stereoview of the experimental electron density from the last round of SHARP/SOLOMAN contoured at 1σ with the final refined N-LIS1 model. The region shown includes Phe31 and surrounding residues.

(B) Stereoview of a Cα trace of the C/D homodimer of N-LIS1 labeled every tenth residue.

(C) The two crystallographically independent homodimers, chain A/B and chain C/D, colored according to the temperature factors, where blue represents low and red high B values. The secondary structure elements are indicated.

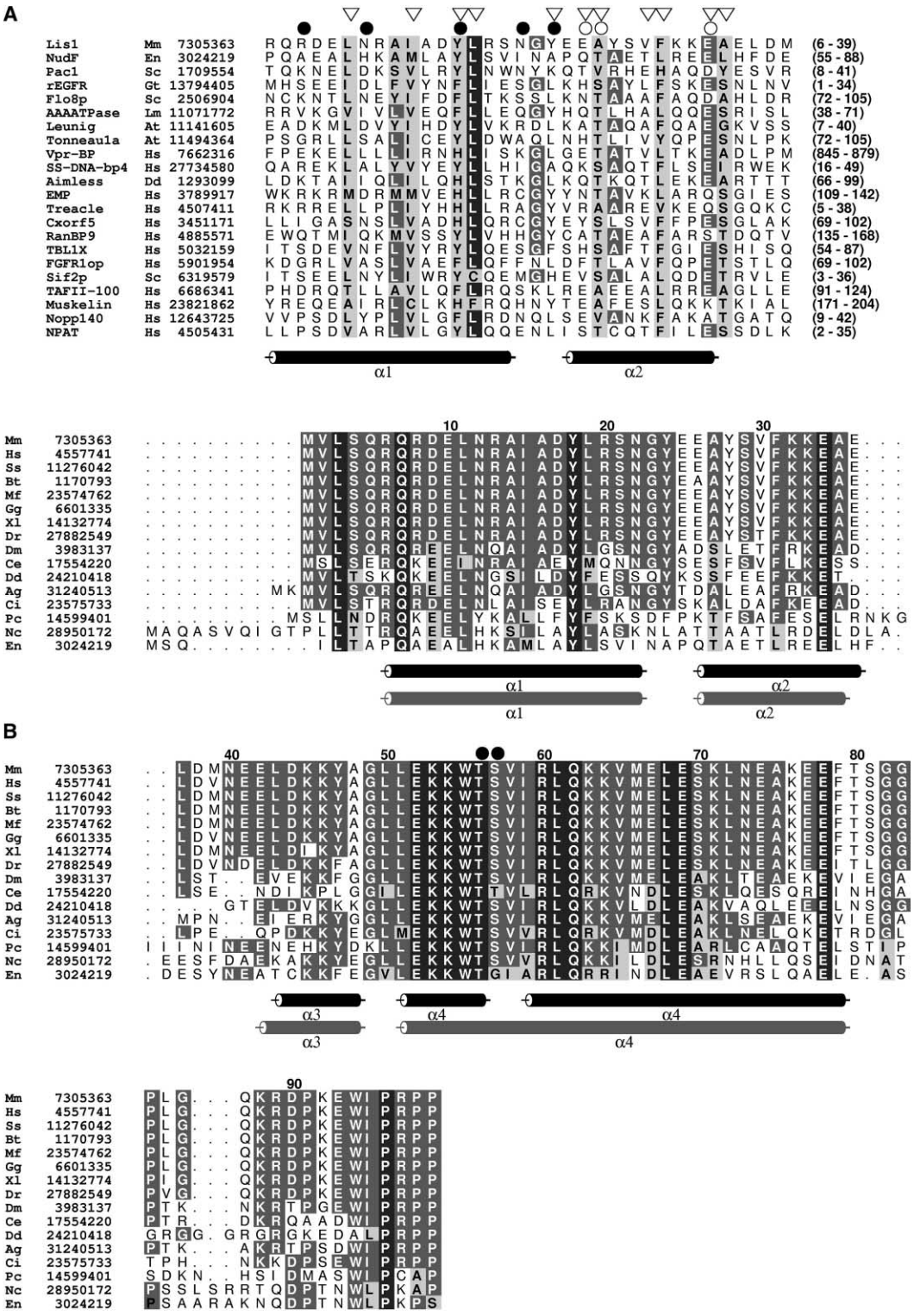

Figure 3. Evolutionary Conservation of LisH Domains

(A) LisH domains from different proteins are aligned to show a topological similarity. Shown beneath the alignments are elements of secondary structure of N-LIS1. Downward arrows represent residues involved in hydrophobic contacts across the dimer interface, closed circles represent residues involved in side chain/side chain hydrogen bonds, and open circles represent residues involved in side chain/main chain hydrogen bonds. Amino acid limits are shown on the right.

(B) Alignment of LIS1 orthologs. The secondary structure elements of each monomer of A/C and B/D are shown in black and gray, respectively. The numbering shown is from the mouse N-LIS1. The two residues located at the conformation altering kink are marked with closed circles. GenBank accession numbers are indicated on the left. Abbreviations: Mm, *Mus musculus*; En, *Emericella nidulans*; Sc, *S. cerevisiae*;

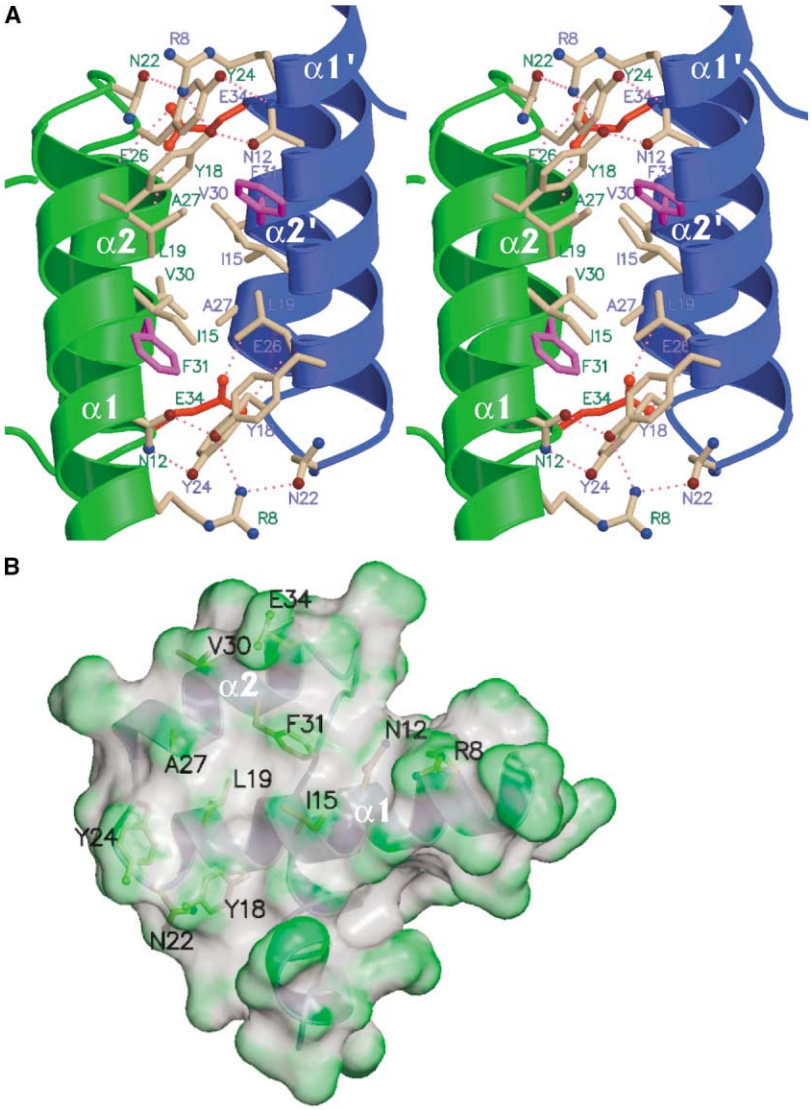

Figure 4. Intermolecular Interface of the Dimmer

(A) A stereo side view between two LisH motifs showing one dimer in green and the other in blue. The most critical side chain contacts involved in the dimer interface are shown. Phe31 is highlighted with purple. The hydrogen bonding network at each end of the interface is shown, as is the helix capping hydrogen bonds of Glu34 in red.

(B) A view of the interface of one monomer represented as a semitransparent surface that is colored by the surface curvature of an isolated monomer.

Discussion

The crystal structure of N-LIS1 reveals for the first time the molecular architecture of a novel and ubiquitous domain, made up by two LisH motifs. The LisH was recently identified in over a hundred eukaryotic proteins. Interestingly, several of these proteins are known to be associated with genetic diseases, and two of these, in addition to LIS1, probably involve defective cell migration: mutations in the *TCOF1* gene coding for the protein treacle cause Treacher-Collins syndrome which involves hearing loss and craniofacial abnormalities (Marszalek et al., 2002), while mutations in the *Cxorf5* gene product cause numerous defects in the central nervous system resulting in lethality in males and an X-linked disorder OFD1 (oral-facial-digital type 1 syndrome) in females characterized by numerous deformations of face, oral cavity, and digits (Ferrante et al., 2003). The function of the LisH motif remains elusive. It has been suggested that it might be involved in self-association, or binding to microtubules, ATPases, or β-propeller domains (Emes and Ponting, 2001), or in some cases even mediate transcriptional activation (Wei et al., 2003).

The notion that LisH serves as a self-association motif is substantiated by some experimental data on LIS1 and its homologs. It has been shown, for example, that LIS1

Gt, *Guillardia theta*; Lm, *Leishmania major*; At, *Arabidopsis thaliana*; Hs, *Homo sapiens*; Dd, *Dictyostelium discoideum*; Ss, *Sus scrofa*; Bt, *Bos Taurus*; Mf, *Macaca fascicularis*; Gg, *Gallus gallus*; Xl, *Xenopus laevis*; Dr, *Danio rerio*; Ce, *C. elegans*; Ag, *Anopheles gambiae*; Ci, *Ciona intestinalis*; Pc, *Pneumocystis carinii*; Nc, *Neurospora crassa*; rEGFR, regulator of epidermal growth factor receptor; Flo8p, transcriptional activator FLO8; Vpr-BP, Vpr binding protein; SS-DNA-bp4, single-stranded DNA binding protein 4; EMP, erythroblast macrophage protein; RanBP9, ran binding protein, TBL1X, transducin β-like 1X; FGFRlop, fibroblast growth factor receptor 1 oncogene partner; Sif2p, Sir4p-Interacting Factor; TAFII-100, Transcription initiation factor TFIID 100 kDa subunit; Nopp140, 140 kDa nucleolar phosphoprotein; NPAT, nuclear protein, ataxia-telangiectasia locus.

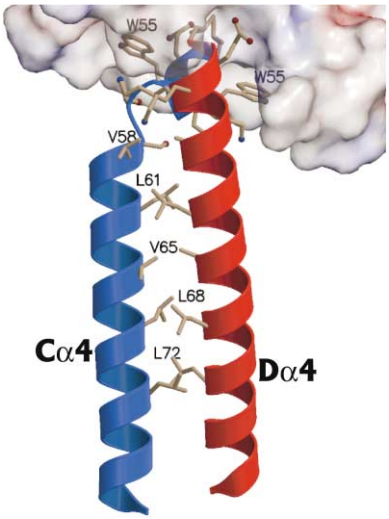

Figure 5. The Coiled-Coil Segment

The coiled coils of C/D dimer are shown as helices extending from a surface of the LisH domain. The hydrophobic residues of the heptad repeats are shown. Surfaces were generated in GRASP (Nicholls et al., 1991).

is a dimer (Garcia-Higuera et al., 1996), and that dimerization is essential for the protein's normal biological function (Cahana et al., 2001). A different investigation showed that the *A. nidulas* ortholog, NudF, must be in the dimeric form to support the growth of the fungus, and the dissociation constant for NudF was measured by ultracentrifugation to be 3.63×10^{-7} M (Ahn and Morris, 2001). Based on subsequent mutagenesis work and qualitative experiments, these authors concluded that the putative coiled-coil region encompassing residues 60–86 is responsible for the dimerization. In contrast, LIS1 fails to dimerize if the N-terminal LisH segment is deleted, leaving the coiled-coil virtually intact (Cahana et al., 2001). A similar observation was reported by Tai et al. (2002). Our work reconciles this apparent contradiction and shows that both LisH and coiled-coil regions contribute to the dimerization effect. We also show that the association of the two LIS1 monomers via the N-LIS1 fragment is thermodynamically very strong, consistent with the large buried surface in each monomer, i.e., 27% of the its total surface.

Of the known five missense mutations of *Lis*1 that have been found in lissencephaly patients, four (H149R, G162S, S169P, and D317H) are found in the β-propeller domain, and one (F31S) in the N-terminal LisH motif. The patient with that mutation suffers from low-severity, grade 4a lissencephaly (Cardoso et al., 2000). Previous research on these mutations indicates that they impact various biochemical and cellular mechanisms, resulting in patients with the diverse lissencephaly phenotypes. In case of F31S, the mutation severely affects the protein's half-life and stability, leads to protein aggregation, and interferes with the ability of LIS1 to interact with its binding partners (Caspi et al., 2003). This structural study allows us to better rationalize the mechanistic implications of the F31S mutation. Phe31 is located in the middle of α_2, with its side chain pointing toward the interior of the LisH domain (Figure 4A). This highly conserved residue (Figure 3B) plays an integral role in the formation of the hydrophobic core and the dimerization interface. The side chain of Phe31 makes intramolecular contacts with Asn12, Ile15, Ala16, and Ala35 and intermolecular contacts with Leu19 and Tyr24. All of these except Ala16 are involved in the dimerization interface. Because of the dimerization of the LisH motif, removing the phenyl ring of F31 would create two hydrophobic cavities in the heart of this dimer, destabilizing the complex. Furthermore, the introduction of a hydrophilic residue at the interface is likely to destroy the integrity of the complex.

The crystal structure of N-LIS1 shows that the prediction of the coiled-coil region downstream of LisH is correct, and indeed such a structure is formed by the three heptad repeat, although it is not clear at this point to what extent this relatively short coiled-coil contributes to the association constant of the two N-LIS1 domains. A surprising observation is that the coiled-coil motif breaks the 2-fold symmetry of the N-LIS1 structure, so that one of the helices contains a kink which aligns the two in a parallel fashion, while they originate at the N termini at a 55° angle. What is particularly interesting is the complete evolutionary conservation of the EKKWT motif which constitutes the N terminus of the α_4 helix. This motif ensures that the two helices of the coiled-coil motif are not parallel in the absence of a significant kink in one of them. From *Pneumocystis carinii* to human, not a single substitution is to be found in this region (Figure 3B). Moreover, the preceding sequence GLL and the downstream motif SVI are almost fully conserved with slight departures in three species of worms and fungi. As this sequence is critical for the initial orientation of the two α_4 helices, it is tempting to speculate that the asymmetry of the dimer has important functional implications (see below).

The presence of the two independent homodimers with nearly identical structure in the asymmetric unit virtually rules out that this phenomenon is due to crystal packing forces. Since the two molecules are equivalent in the dimer, if the two WD40 domains of LIS1 are fixed, the head (LisH) can swivel between the two alternative positions by about 50°. This is reminiscent of motions observed in molecular motors, although no such function was ever implied for LIS1. It is possible that such flexibility is required to accommodate motions associated with dynein-mediated structural changes. It is also possible that the two dimerization regions are used alternately in the cell, based on physiological state. Thus, the molecule could exist in either open or closed scissor conformations. Further studies to clarify this point are in progress in our laboratories.

Protein Expression and Purification

The mouse N-LIS1 fragment (residues 1–86) was subcloned into the NcoI and XhoI sites of the pGSTUni1 expression vector (Sheffield et al., 1999). The methionine auxotroph *E. coli* B834 (DE3) (Novagen) was transformed with the expression plasmid. Protein was expressed in minimal medium supplemented with 50 mg ml^{-1} SeMet by overnight induction with 1 mM IPTG at 25°C. The SeMet-substituted N-LIS1 was purified by glutathione affinity chromatography (Pharmacia) followed by the re-

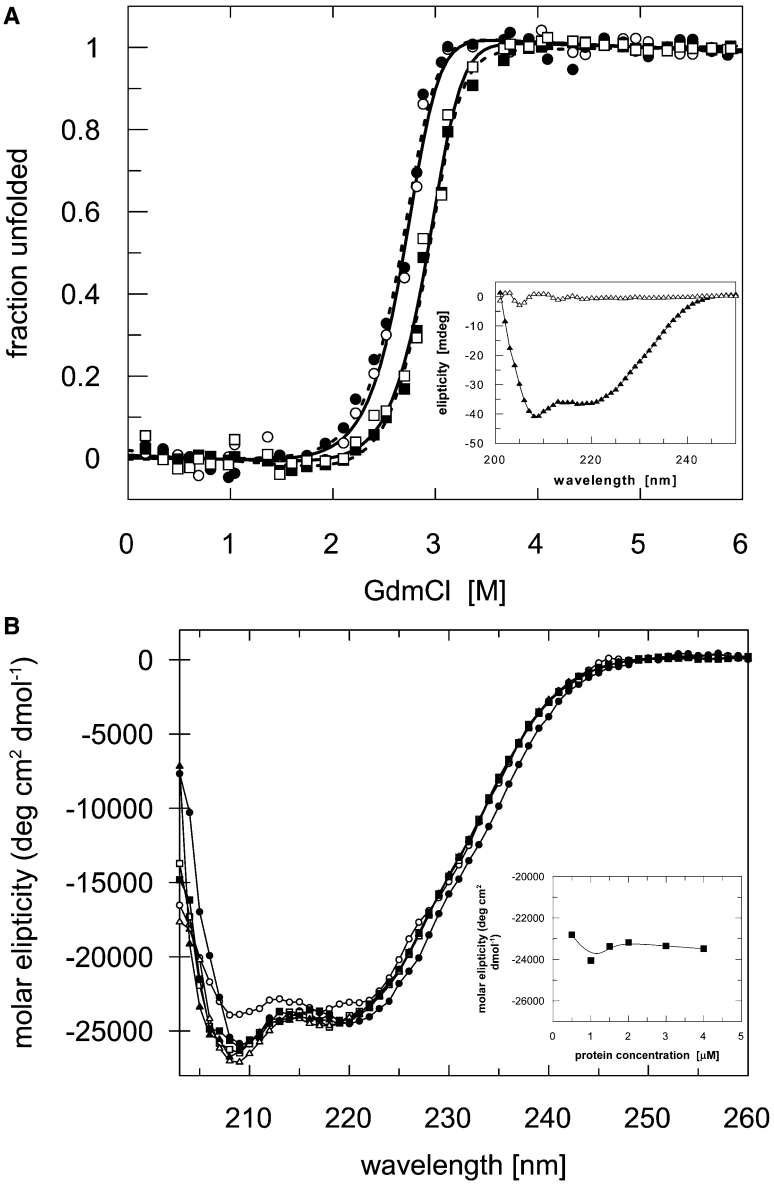

Figure 6. Thermodynamics of N-LIS1 Homodimerization

(A) GdmCl-induced unfolding transitions of LIS1 at 0.25 μM (circles) and at 3 μM (squares) monitored by fluorescence at 341 nm (white circles) and far-UV CD at 222 nm (black circles). All curves were fitted to a two-state dimer denaturation model as described in Experimental Procedures; fit to CD data (dashed line), fit to fluorescence data (continous black line). The inset shows CD signal of 2.5 μM LIS1 in the absence of GdmCl (black triangles) and in 6 M GdmCl (white triangles).

(B) CD spectra of Lis-1 (1-86) at different protein concentrations: 0.5 μM (white circles), 1 μM (black circles), 1.5 μM (white squares), 2 μM (black squares), 3 μM (white triangles), and 4 μM (black triangles). The inset presents molar elipticity CD signal as a function of LIS1 concentration range at 222 nm.

moval of the GST tag with the rTEV protease, and final purification was on a Superdex 75 gel filtration column (Pharmacia). The purified protein was dialyzed against 50 mM Tris-HCl (pH 7.0) and 1 mM DTT, and concentrated to 10 mg ml^{-1}.

Crystallization and Data Collection

The crystals were grown by the sitting-drop vapor-diffusion technique under mineral oil at 21°C, by mixing equal volumes of the protein solution and the reservoir solution which contained 1.7 M $(NH_4)_2SO_4$ and 0.1 M Na_3-citrate (pH 4.5). The crystals belong to space group $P2_12_12$ with unit cell dimensions a = 63.0 Å, b = 111.7 Å, and c = 47.4 Å. The Matthew's coefficient assuming four copies of N-LIS1 in the asymmetric unit is 2.1 $Å^3$/Da, which corresponds to 40.1% solvent. The crystals were flash frozen in a solution containing 2.4 M $(NH_4)_2SO_4$, 0.1 M Na_3-citrate (pH 4.5), and 20% glycerol. In situ flash-

Table 2. Thermodynamic Parameters for the GdmCl-Induced Unfolding of N-LIS1

[N-LIS1]	0.25 μM		0.5 μM		1.5 μM		3 μM	
	FL at 341 nm	CD at 222 nm	FL at 341 nm	CD at 222 nm	FL at 341 nm	CD at 222 nm	FL at 341 nm	CD at 222 nm
$[GdmCl]_{1/2}$ (M)	2.7	2.68	2.79	2.8	2.84	2.89	2.93	2.92
m (kcal/mol/M)	4.99	4.92	4.72	5.1	5.12	5.19	4.93	4.85
ΔG_U^{H2O} (kcal/mol)	22.444	22.109	21.685	23.063	22.469	22.958	21.925	21.638

annealing method (Harp et al., 1998) was applied to improve the diffraction quality of the crystals. Data were collected from a SeMet-labeled crystal at the Southeast Regional Collaborative Access Team (SER-CAT) 22-ID beamline at the Advanced Photon Source, Argonne National Laboratory. Data were collected to 1.75 Å resolution at 0.97939 Å (peak wavelength), 0.97953 Å (edge wavelength), and 0.96422 Å (high-energy remote), and processed with HKL2000 (Otwinowski and Minor, 1997). Two wedges of 180° were collected at the inflection point and high-energy wavelengths, and a single wedge of 180° was collected for the peak wavelength. Data collection and processing statistics are presented in Table 1.

Structure Determination

The program SOLVE (Terwilliger and Berendzen, 1999) was used to locate six of the eight Se atoms in the asymmetric unit and to calculate initial phases using data to 2.3 Å from the first 180° wedges of all three wavelength data sets and using values of f' and f'' estimated from the X-ray fluorescence scans. RESOLVE (Terwilliger, 2003) was able to build 179 of the expected 352 residues (50.8%), and this partial model was used as a starting point for ARP/WARP (Perrakis et al., 1999) which added main chain atoms for the additional 61 amino acids. The phases based on the resulting model were used to calculate anomalous difference maps and to locate the remaining two selenium atoms. The programs SHARP (de La Fortelle and Bricogne, 1997), SOLOMON (Abrahams and Leslie, 1996), and ARP/WARP were then used to improve the maps and extend the model. Manual model building in O (Jones et al., 1991) was used to generate the rest of the model, with the help of a noncrystallographic correlation mask using COMA (Kleywegt, 1999) followed by NCS averaging in AVE (Kleywegt and Read, 1997). The final model contains 311 residues (88.4% of the expected number), 183 waters, 4 sulfate ions, 1acetate, and 1 benzoic acid. The source of the benzoic acid is unclear, and its assignment is based entirely on the residual electron density which perfectly fits that entity. Refinement was performed in REFMAC5.1 (Murshudov et al., 1997) with maximum likelihood residuals used throughout the process. Noncrystallographic symmetry was used during early rounds of refinement. TLS refinement and experimental phase information from SOLVE were included in later stages of refinement. MOLPROBITY and OOPS2 (Kleywegt, 2000) were used as a validation tools. Refinement data are presented in Table 1.

Chemical Unfolding

The guanidinium chloride (GdmCl)-induced unfolding reactions of N-LIS1 were monitored by steady-state fluorescence and CD spectroscopy. Ultrapure GdmCl (ICN Biochemicals, Inc.) was used for 6 M stock preparation in 20 mM phosphate, 150 mM NaCl, pH 7.4. A range of GdmCl concentrations was prepared by stock dilutions, filtered, and measured with a refractometer (Carl Zeiss). For denaturation experiments, protein samples were incubated at increasing concentrations of GdmCl and equilibrated for 12 hr. Fluorescence emission measurements were carried out in 1 cm cells using a FP-750 spectrofluorimeter (Jasco) equipped with an ETC-272 Peltier temperature controller (Jasco). The samples were excited at 280 nm and emission was measured at 341 nm. Fluorescence signal from each sample was averaged from five measurements (5 nm excitation and emission band widths with the response time 8 s). Circular dichroism (CD) spectra were collected with a J-715 spectropolarimeter (Jasco) using a 2 nm band width and response time of 4 s. The CD spectra were recorded as the average of three scans obtained between 200 and 260 nm at the rate 50 nm/minute. The spectra recorded at various protein concentrations were converted to a mean residue molar elipticity. All the experiments were performed at 25°C.

The denaturation profiles of N-LIS1 obtained by fluorescence and CD methods at various protein concentrations were normalized and analyzed according to a two-state dimer denaturation model: $N_2 \leftrightarrow 2\ D$, with N_2 describing native dimer and D, denatured monomer. The equilibrium constant of unfolding (K_U) was calculated according to Neet and Timm (1994). The standard denaturation parameters, $[GdmCl]_{1/2}$, m, and $\Delta G_u^{H_2O}$ were determined by fitting individual data sets to an equation given by Mateu (2002). The analysis of the data was performed by the program GraFit (Erithacus Software Ltd.).

Acknowledgments

This work was supported by NIH grant NS36267 (to Z.S.D.). Data were collected at Southeast Regional Collaborative Access Team (SER-CAT) 22-ID beamline at the Advanced Photon Source (APS), Argonne National Laboratory. Use of the APS is supported by the US Department of Energy, Office of Science, Office of Basic Energy Sciences, under Contract No. W-31-109-Eng-38. This work was supported in part by a March of Dimes Grant 6-FY01-5, (to O.R.). We thank Natalya Olekhnovich for excellent technical assistance and the staff of SER-CAT for help with data collection. J.O. thanks HHMI for generous support.

Received: January 12, 2004
Revised: February 26, 2004
Accepted: March 5, 2004
Published: June 8, 2004

References

Abrahams, J.P., and Leslie, A.G.W. (1996). Methods used in the structure determination of bovine mitochondrial F1 ATPase. Acta Crystallogr. D *52*, 30–42.

Ahn, C., and Morris, N.R. (2001). Nudf, a fungal homolog of the human LIS1 protein, functions as a dimer *in vivo*. J. Biol. Chem. *276*, 9903–9909.

Albrecht, U., Abu-Issa, R., Ratz, B., Hattori, M., Aoki, J., Arai, H., Inoue, K., and Eichele, G. (1996). Platelet-activating factor acetylhydrolase expression and activity suggests a link between neuronal migration and platelet-activating factor. Dev. Biol. *180*, 579–593.

Berg, M.J., Schifitto, G., Powers, J.M., Martinez-Capolino, C., Fong, C.T., Myers, G.J., Epstein, L.G., and Walsh, C.A. (1998). X-linked female band heterotopia-male lissencephaly syndrome. Neurology *50*, 1143–1146.

Bowie, J.U., and Sauer, R.T. (1989). Equilibrium dissociation and unfolding of the Arc repressor dimer. Biochemistry *28*, 7139–7143.

Cahana, A., Escamez, T., Nowakowski, R.S., Hayes, N.L., Giacobini, M., von Holst, A., Shmueli, O., Sapir, T., McConnell, S.K., Wurst, W., et al. (2001). Targeted mutagenesis of Lis1 disrupts cortical

development and LIS1 homodimerization. Proc. Natl. Acad. Sci. USA *98*, 6429–6434.

Cardoso, C., Leventer, R.J., Matsumoto, N., Kuc, J.A., Ramocki, M.B., Mewborn, S.K., Dudlicek, L.L., May, L.F., Mills, P.L., Das, S., et al. (2000). The location and type of mutation predict malformation severity in isolated lissencephaly caused by abnormalities within the LIS1 gene. Hum. Mol. Genet. *9*, 3019–3028.

Caspi, M., Coquelle, F.M., Koifman, C., Levy, T., Arai, H., Aoki, J., De Mey, J.R., and Reiner, O. (2003). LIS1 missense mutations: variable phenotypes result from unpredictable alterations in biochemical and cellular properties. J. Biol. Chem. *278*, 38740–38748.

Coquelle, F.M., Caspi, M., Cordelières, F.P., Dompierre, J.P., Dujardin, D.L., Koifman, C., Martin, P., Hoogenraad, C.C., Akhmnanova, A., Galjart, N., et al. (2002). LIS1, CLIP-170's key to the dynein/dynactin pathway. Mol. Cell. Biol. *22*, 3089–3102.

Dawe, A.L., Caldwell, K.A., Harris, P.M., Morris, N.R., and Caldwell, G.A. (2001). Evolutionarily conserved nuclear migration genes required for early embryonic development in *Caenorhabditis elegans*. Dev. Genes Evol. *211*, 434–441.

de La Fortelle, E., and Bricogne, G. (1997). Maximum-likelihood heavy atom parameter refinement for multiple isomorphous replacement and multiwavelength anomalous diffraction methods. Methods Enzymol. *276*, 472–494.

des Portes, V., Pinard, J.M., Billuart, P., Vinet, M.C., Koulakoff, A., Carrie, A., Gelot, A., Dupuis, E., Motte, J., Berwald-Netter, Y., et al. (1998). A novel CNS gene required for neuronal migration and involved in X-linked subcortical laminar heterotopia and lissencephaly syndrome. Cell *92*, 51–61.

Emes, R.D., and Ponting, C.P. (2001). A new sequence motif linking lissencephaly, Treacher Collins and oral-facial-digital type 1 syndromes, microtubule dynamics and cell migration. Hum. Mol. Genet. *10*, 2813–2820.

Faulkner, N.E., Dujardin, D.L., Tai, C.Y., Vaughan, K.T., O'Connell, C.B., Wang, Y., and Vallee, R.B. (2000). A role for the lissencephaly gene LIS1 in mitosis and cytoplasmic dynein function. Nat. Cell Biol. *2*, 784–791.

Feng, Y., Olson, E.C., Stukenberg, P.T., Flanagan, L.A., Kirschner, M.W., and Walsh, C.A. (2000). LIS1 regulates CNS lamination by interacting with mNudE, a central component of the centrosome. Neuron *28*, 665–679.

Ferrante, M.I., Barra, A., Truong, J.P., Banfi, S., Disteche, C.M., and Franco, B. (2003). Characterization of the OFD1/Ofd1 genes on the human and mouse sex chromosomes and exclusion of Ofd1 for the Xpl mouse mutant. Genomics *81*, 560–569.

Francis, F., Koulakoff, A., Boucher, D., Chafey, P., Schaar, B., Vinet, M.C., Friocourt, G., McDonnell, N., Reiner, O., Kahn, A., et al. (1999). Doublecortin is a developmentally regulated, microtubule-associated protein expressed in migrating and differentiating neurons. Neuron *23*, 247–256.

Garcia-Higuera, I., Fenoglio, J., Li, Y., Lewis, C., Panchenko, M.P., Reiner, O., Smith, T.F., and Neer, E.J. (1996). Folding of proteins with WD-repeats: comparison of six members of the WD-repeat superfamily to the G protein beta subunit. Biochemistry *35*, 13985–13994.

Geiser, J.R., Schott, E.J., Kingsbury, T.J., Cole, N.B., Totis, L.J., Bhattacharyya, G., He, L., and Hoyt, M.A. (1997). Saccharomyces cerevisiae genes required in the absence of the CIN8-encoded spindle motor act in functionally diverse mitotic pathways. Mol. Biol. Cell *8*, 1035–1050.

Gibrat, J.F., Madej, T., and Bryant, S.H. (1996). Surprising similarities in structure comparison. Curr. Opin. Struct. Biol. *6*, 377–385.

Gleeson, J.G., Allen, K.M., Fox, J.W., Lamperti, E.D., Berkovic, S., Scheffer, I., Cooper, E.C., Dobyns, W.B., Minnerath, S.R., Ross, M.E., et al. (1998). Doublecortin, a brain-specific gene mutated in human X-linked lissencephaly and double cortex syndrome, encodes a putative signaling protein. Cell *92*, 63–72.

Gleeson, J.G., Lin, P.T., Flanagan, L.A., and Walsh, C.A. (1999). Doublecortin is a microtubule-associated protein and is expressed widely by migrating neurons. Neuron *23*, 257–271.

Gruber, M., and Lupas, A.N. (2003). Historical review: another 50th anniversary—new periodicities in coiled coils. Trends Biochem. Sci. *28*, 679–685.

Harp, J.M., Timm, D.E., and Bunick, G.J. (1998). Macromolecular crystal annealing: overcoming increased mosaicity associated with cryocrystallography. Acta Crystallogr. D *54*, 622–628.

Hattori, K., Adachi, H., Matsuzawa, A., Yamamoto, K., Tsujimoto, M., Aoki, J., Hattori, M., Arai, H., and Inoue, K. (1996). cDNA cloning and expression of intracellular platelet-activating factor (PAF) acetylhydrolase II. J. Biol. Chem. *271*, 33032–33038.

Holm, L., and Sander, C. (1997). Dali/FSSP classification of three-dimensional protein folds. Nucleic Acids Res. *25*, 231–234.

Horesh, D., Sapir, T., Francis, F., Wolf, S.G., Caspi, M., Elbaum, M., Chelly, J., and Reiner, O. (1999). Doublecortin, a stabilizer of microtubules. Hum. Mol. Genet. *8*, 1599–1610.

Jones, T.A., Zou, J.Y., Cowan, S.W., and Kjeldgaard, M. (1991). Improved methods for binding protein models in electron density maps and the location of errors in these models. Acta Crystallogr. A *47*, 110–119.

Kim, M.H., Cierpicki, T., Derewenda, U., Krowarsch, D., Feng, Y., Devedjiev, Y., Dauter, Z., Walsh, C.A., Otlewski, J., Bushweller, J.H., et al. (2003). The DCX-domain tandems of doublecortin and doublecortin-like kinase. Nat. Struct. Biol. *10*, 324–333.

Kitagawa, M., Umezu, M., Aoki, J., Koizumi, H., Arai, H., and Inoue, K. (2000). Direct association of LIS1, the lissencephaly gene product, with a mammalian homologue of a fungal nuclear distribution protein, rNUDE. FEBS Lett. *479*, 57–62.

Kleywegt, G.J. (1999). Experimental assessment of differences between related protein crystal structures. Acta Crystallogr. D *55*, 1878–1884.

Kleywegt, G.J. (2000). Validation of protein crystal structures. Acta Crystallogr. D *56*, 249–265.

Kleywegt, G.J., and Read, R.J. (1997). Not your average density. Structure *5*, 1557–1569.

Lovell, S.C., Davis, I.W., Arendall, W.B., de Bakker, P.I.W., Word, J.M., Prisant, M.G., Richardson, J.S., and Richardson, D.C. (2002). Structure validation by Calpha geometry: phi, psi and Cbeta deviation. Proteins *50*, 437–450.

Mateu, M.G. (2002). Conformational stability of dimeric and monomeric forms of the C-terminal domain of human immunodeficiency virus-1 capsid protein. J. Mol. Biol. *318*, 519–531.

Marszalek, B., Wojcicki, P., Kobus, K., and Trzeciak, W.H. (2002). Clinical features, treatment and genetic background of Treacher Collins syndrome. J. Appl. Genet. *43*, 223–233.

Morris, R. (2000). A rough guide to a smooth brain. Nat. Cell Biol. *2*, E201–E202.

Murshudov, G.N., Vagin, A.A., and Dodson, E.J. (1997). Refinement of macromolecular structures by the maximum-likelihood Method. Acta Crystallogr. D Biol. Crystallogr. *53*, 240–255.

Nayernia, K., Vauti, F., Meinhardt, A., Cadenas, C., Schweyer, S., Meyer, B.I., Schwandt, I., Chowdhury, K., Engel, W., and Arnold, H.H. (2003). Inactivation of a testis-specific Lis1 transcript in mice prevents spermatid differentiation and causes male infertility. J. Biol. Chem. *278*, 48377–48385.

Neer, E.J., Schmidt, C.J., Nambudripad, R., and Smith, T.F. (1994). The ancient regulatory protein family of WD-repeat proteins. Nature *371*, 297–300.

Neet, K.E., and Timm, D.E. (1994). Conformational stability of dimeric proteins: quantitative studies by equilibrium denaturation. Protein Sci. *3*, 2167–2174.

Nicholls, A., Sharp, K., and Honig, B. (1991). Protein folding and association: insights from the interfacial and thermodynamic properties of hydrocarbons. Proteins *11*, 281–296.

Niethammer, M., Smith, D.S., Ayala, R., Peng, J., Ko, J., Lee, M., Morabito, M., and Tsai, L. (2000). NUDEL is a novel Cdk5 substrate that associates with LIS1 and cytoplasmic dynein. Neuron *28*, 697–711.

Otwinowski, Z., and Minor, W. (1997). Processing of X-ray diffraction

data collected in oscillation mode. Methods Enzymol. A *276*, 307–326.

Payne, C., St John, J.C., Ramalho-Santos, J., and Schatten, G. (2003). LIS1 association with dynactin is required for nuclear motility and genomic union in the fertilized mammalian oocyte. Cell Motil. Cytoskeleton *56*, 245–251.

Perrakis, A., Morris, R., and Lamzin, V.S. (1999). Automated protein model building combined with iterative structure refinement. Nat. Struct. Biol. *6*, 458–463.

Reiner, O., Carrozzon, R., Shen, Y., Wehnert, M., Faustinella, F., Dobyns, W.B., Caskey, C.T., and Ledbetter, D.H. (1993). Isolation of a Miller-Dieker lissencephaly gene containing G-protein β-subunits-like repeats. Nature *364*, 717–721.

Ross, M.E., and Walsh, C.A. (2001). Human brain malformations and their lessons for neuronal migration. Annu. Rev. Neurosci. *24*, 1041–1070.

Sapir, T., Elbaum, M., and Reiner, O. (1997). Reduction of microtubule catastrophe events by LIS1, platelet-activating factor acetylhydrolase subunit. EMBO J. *16*, 6977–6984.

Sapir, T., Horesh, D., Caspi, M., Atlas, R., Burgess, H.A., Wolf, S.G., Francis, F., Chelly, J., Elbaum, M., Pietrokovski, S., et al. (2000). Doublecortin mutations cluster in evolutionarily conserved functional domains. Hum. Mol. Genet. *9*, 703–712.

Sasaki, S., Shionoya, A., Ishida, M., Gambello, M.J., Yingling, J., Wynshaw-Boris, A., and Hirotsune, S. (2000). A LIS1/NUDEL/cytoplasmic dynein heavy chain complex in the developing and adult nervous system. Neuron *28*, 681–696.

Sheffield, P., Garrard, S., and Derewenda, Z. (1999). Overcoming expression and purification problems of RhoGDI using a family of "Parallel" expression vectors. Protein Expr. Purif. *15*, 34–39.

Sheffield, P.J., Garrard, S., Caspi, M., Aoki, J., Arai, H., Derewenda, U., Inoue, K., Suter, B., Reiner, O., and Derewenda, Z.S. (2000). Homologs of the alpha- and beta-subunits of mammalian brain platelet-activating factor acetylhydrolase Ib in the Drosophila melanogaster genome. Proteins *39*, 1–8.

Smith, D.S., Niethammer, M., Ayala, R., Zhou, Y., Gambello, M.J., Wynshaw-Boris, A., and Tsai, L.H. (2000). Regulation of cytoplasmic dynein behaviour and microtubule organization by mammalian Lis1. Nat. Cell Biol. *2*, 767–775.

Tai, C.-Y., Dujardin, D.L., Faulkner, N.E., and Vallee, R.B. (2002). Role of dynein, dynactin, and CLIP-170 interactions in LIS1 kinetochore function. J. Cell Biol. *156*, 959–968.

Taylor, K.R., Holzer, A.K., Bazan, J.F., Walsh, C.A., and Gleeson, J.G. (2000). Patient mutations in doublecortin define a repeated tubulin-binding domain. J. Biol. Chem. *275*, 34442–34450.

Terwilliger, T.C. (2003). Automated side-chain model building and sequence assignment by template matching. Acta Crystallogr. D *59*, 45–49.

Terwilliger, T.C., and Berendzen, J. (1999). Automated MAD and MIR structure solution. Acta Crystallogr. D Biol. Crystallogr. *55*, 849–861.

Tokuoka, S.M., Ishii, S., Kawamura, N., Satoh, M., Shimada, A., Sasaki, S., Hirotsune, S., Wynshaw-Boris, A., and Shimizu, T. (2003). Involvement of platelet-activating factor and LIS1 in neuronal migration. Eur. J. Neurosci. *18*, 563–570.

Wei, Y., Jin, J., and Harper, J.W. (2003). The cyclin E/Cdk2 substrate and Cajal body component p220(NPAT) activates histone transcription through a novel LisH-like domain. Mol. Cell. Biol. *23*, 3669–3680.

Xiang, X., Osmani, A.H., Osmani, S.A., Xin, M., and Morris, N.R. (1995). NudF, a nuclear migration gene in *Aspergillus nidulans* is similar to the human *LIS-1* gene required for neuronal migration. Mol. Biol. Cell *6*, 297–310.

Accession Numbers

The atomic coordinates of N-LIS1 were deposited in the PDB as entry 1uuj, with the corresponding structure factors deposited as r1uujsf.